

COVID-19 detection using Residual Attention Network an Artificial Intelligence approach

Vishal Sharma
Department of Computer Science
Utah State University
vishal.sharma@usu.edu

Curtis Dyreson
Department of Computer Science
Utah State University
curtis.dyreson@usu.edu

ABSTRACT

Coronavirus Disease 2019 (COVID-19) is caused by the severe acute respiratory syndrome coronavirus 2 virus (SARS-CoV-2). The virus transmits rapidly, it has a basic reproductive number (R_0) of 2.2–2.7. In March, 2020 the World Health Organization declared the COVID-19 outbreak a pandemic. Effective testing for COVID-19 is crucial to controlling the outbreak since infected patients can be quarantined. But the demand for testing outstrips the availability of test kits that use Reverse Transcription Polymerase Chain Reaction (RT-PCR). In this paper, we present a technique to detect COVID-19 using Artificial Intelligence. Our technique takes only a few seconds to detect the presence of the virus in a patient. We collected a dataset of chest X-ray images and trained several popular deep convolution neural network-based models (VGG, MobileNet, Xception, DenseNet, InceptionResNet) to classify chest X-rays. Unsatisfied with these models we then designed and built a Residual Attention Network that was able to detect COVID-19 with a testing accuracy of 98% and a validation accuracy of 100%. Feature maps of our model show which areas within a chest X-ray are important for classification. Our work can help to increase the adaptation of AI-assisted applications in clinical practice.

1 INTRODUCTION

In February 2003 some people in Guangdong province in China became infected with a severe acute respiratory syndrome virus (SARS-CoV) [32]. Eventually SARS was detected in about 8000 patients across 26 countries, and the World Health Organization (WHO) reported 774 deaths due to SARS [27]. In September 2012, a similar incident happened with the Middle East respiratory syndrome virus (MERS-CoV). There were 2494 confirmed cases of infection with 858 deaths due to MERS-CoV [28].

Both SARS and MERS pale in significance to the latest CoV outbreak with respect to human health. In November 2019 pneumonia-like cases due to unknown causes started to appear in Wuhan, China killing hundreds of people in the initial weeks. In early 2020, the International Committee on the Taxonomy of Viruses (ICTV) declared the virus as Coronavirus disease 2019 (COVID-19) caused by the SARS-CoV-2 virus [32]. The reproductive number (R_0) of

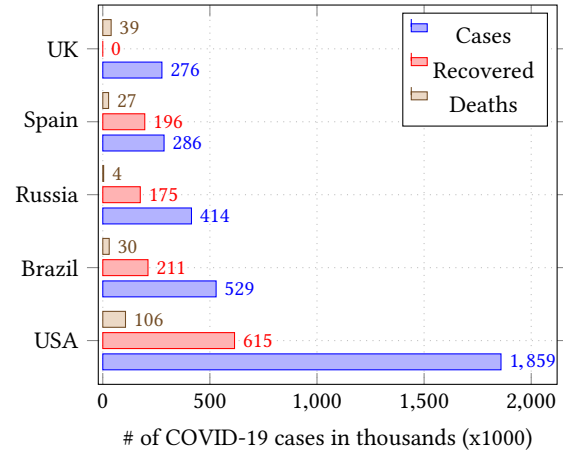


Figure 1: Top 5 countries COVID-19 cases count (UK did not report recovered cases) as of June 1, 2020

COVID-19 is 2.2 – 2.7 [33] higher than SARS coronavirus because of an S protein in the RBD region of SARS-CoV-2 [30]. The highly transmissible virus quickly spread globally. By June 1, 2020 COVID-19 had been detected in 212 countries with five and a half million cases and three hundred and fifty thousand deaths. Figure 1 shows the number of COVID-19 cases, recovered cases, and deaths from COVID-19 in five countries with high rates of infection. On March 11, 2020 WHO characterized COVID-19 as a pandemic.

Diagnosing who has COVID-19 can help curb its spread by quarantining those infected. Currently, the most widely used technique for detecting COVID-19 is with viral nucleic acid detection using Reverse Transcription Polymerase Chain Reaction (RT-PCR), which works by detecting viral RNA from sputum or a nasopharyngeal swab [40]. Unfortunately, there is a shortage of RT-PCR test kits [24]. RT-PCR are also relatively slow, a test takes at best about four hours to complete, even in a highly controlled environment. And RT-PCR tests have a high false positive rate (about 30%) [41].

Recent advances in the field of computer vision suggest the possibility of a faster, widely available alternative for detecting COVID-19. A common symptom of COVID-19 patients is difficulty breathing [32, 46]. A CT scan of a patient's chest has shown higher accuracy and sensitivity than a RT-PCR test for COVID-19 detection [1]. Another study [17] further validates at least 20% higher detection sensitivity from CT scans versus RT-PCR tests. Identifying who has COVID-19 using an imaging technique is (relatively) non-intrusive, uses widely-available (in the developed world) X-ray or CT scanners, and can be used at a very early stage to diagnose COVID-19 and limit the spread of the virus [43].

Permission to make digital or hard copies of all or part of this work for personal or classroom use is granted without fee provided that copies are not made or distributed for profit or commercial advantage and that copies bear this notice and the full citation on the first page. Copyrights for components of this work owned by others than ACM must be honored. Abstracting with credit is permitted. To copy otherwise, or republish, to post on servers or to redistribute to lists, requires prior specific permission and/or a fee. Request permissions from permissions@acm.org.

Conference'17, July 2017, Washington, DC, USA

© 2020 Association for Computing Machinery.

ACM ISBN 978-x-xxxx-xxxx-x/YY/MM... \$15.00

<https://doi.org/10.1145/nnnnnnn.nnnnnnn>

Deep neural networks have been successful in processing medical images [44] and image processing in general, for instance in object detection [35], image segmentation [4], and image classification [19]. Among deep learning techniques, convolutional neural networks (CNN) are popular for processing medical images, *e.g.*, for classification [21] and segmentation [18]. Advances in CNN models over the past few years have led to robust implementations such as VGGNet [23], Inception [34], DenseNet [16], Xception [9], and MobileNet [15]. Recently, Attention Mechanism [37] which generates attention-aware features based on spatial features has become popular in the fields of computer vision and image processing. Attention Mechanism has been deployed on several types of neural networks such as CNN [38], LSTM [5], and Generative Adversarial Networks [45].

In this paper, we report on experiments with various deep learning models to detect and classify COVID-19 from chest X-Ray images of patients. The models we use are VGG, ResNet, MobileNet, DenseNet, Xception, Attention and Residual based CNN (Residual Attention Network). We first collected X-ray images of COVID-19 patients and people without the disease, which we call the “normal” class. Note that the normal class can have other illnesses, such as pneumonia. This image dataset is from a diverse population in terms of location, age, and gender. To better understand the dataset we analyzed it with a popular non-linear dimensionality reduction technique, UMAP. The reduction produces a clear distinction between those with COVID-19 and those without as shown in Figure 2. Next we split the dataset into training, testing and validation sets. We configured several deep learning models for optimal results and trained the models on the dataset. To improve the modeling we designed and built our own Residual Attention Network with better feature extraction using custom designs of residual and attention block. Our model outperforms other models with 98% on the test set and 100% accuracy on the validation set. We extracted feature maps from our model and observed the Residual Attention Network detecting potential COVID-19 infected areas. The major challenge in this research is developing an effective model using only a very small dataset. In summary, this paper makes the following contributions:

- a novel dataset of curated images for use in COVID-19 research,
- a problem-specific, highly accurate classification model using Residual Connection and Attention Mechanism,
- an explainable diagnosis using feature maps, and
- a reproducible dataset and classifier, all of our code and data is in the public domain.

This paper is organized as follows. Section 2 outlines related work and potential limitations. Section 3 describes our dataset collection and basic analysis. Section 4 describes our approach and modifications of the Residual Attention Network. Section 5 shows experimental configurations and reports the results of several experiments, and finally Section 6 presents conclusions and future work.

2 RELATED WORK

There are over 24,000 research papers on COVID-19 from well known sources like *bioRxiv*, *arXiv* and *medRxiv* out of which more

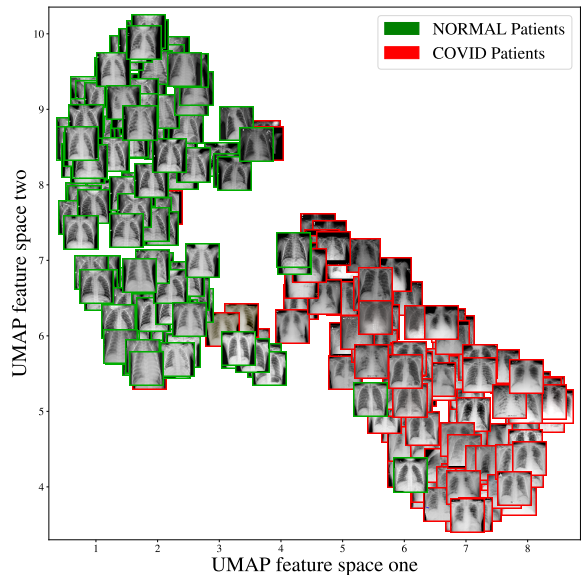


Figure 2: UMAP features of chest X-ray images of patients in our dataset

than 1,500 are peer reviewed [29]; there are even two recent review papers about using AI techniques in COVID-19 detection [31, 42]. We focus on research that uses deep learning for COVID-19 detection. Wang et al. [39] use 1,065 chest CT scan images of COVID-19 patients to build a classifier using InceptionNet. They report an accuracy of 89.5%, a specificity of 0.88, and a sensitivity of 0.87. Xu et al. [7] use 3D Convolution Neural Networks (CNNs) and report an accuracy of 86.7%. Chen et al. [8] segment the infected areas in CT scans using UNet++ [47]. Using transfer learning and pre-defined models to classify COVID-19 in CT scans has also been researched, for instance using DenseNet [16] *e.g.*, [20, 22], ResNet [14] *e.g.*, [13, 26], and CNN *e.g.*, [3, 13, 20]. Traditional machine learning (ML) methods of feature extraction and conventional ML algorithms for classification have also been used. Mucahid et al. [6] use feature extraction techniques GLCM, LDP, GLRLM and DWT, and pass extracted features to a Support Vector Machine (SVM) for classification. They report an accuracy of 99.68% in the best configuration settings. Alqudah et al. [2] apply various ML techniques, such as SVM and Random Forest, and report an accuracy of 95%.

To the best of our knowledge we are the first to use Residual Attention Mechanism [37] to extract spatial-aware features and perform classification of a COVID-19 dataset. We obtained higher test and validation accuracy, precision, recall, sensitivity and specificity than previous work. Additionally, most of the previous research used more sophisticated CT scan images which usually take 20 to 30 minutes to perform, but we use X-ray images which are faster to extract, about 10 minutes in most cases. X-ray machines are more widely available than CT scanners, and there are portable X-ray units that can be deployed anywhere, not just in medical facilities.

3 DATASET

We collected images only from public sources, which provide the data while maintaining patients’ privacy. The dataset of COVID-19 X-ray images comes from radiopaedia.org¹, the website of the

¹radiopaedia.org

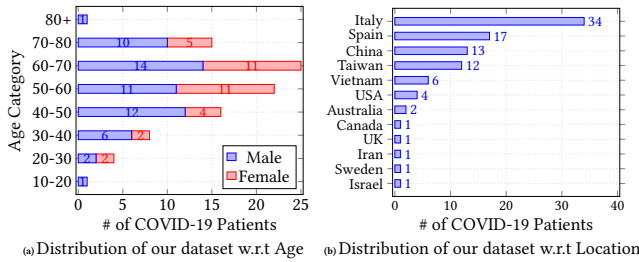


Figure 3: Distribution of our dataset with positive COVID-19 based on location, gender and age

Italian society of medical and interventional radiology². Cohen et al. [11] scraped the images from the website using PDF processing tools. We selected 120 images of patients with COVID-19, specifically we selected all *Posterioranterior* (PA) images. The PA view has an anterior aspect in which the ribs are much clearer than the *Anteriorposterior* or *Lateral* view X-ray. To collect images of non-COVID-19 (which we call normal) chests we randomly selected images from a repository collected by Mooney et al. [25]. In this repository there are chest X-ray images of patients with pneumonia and regular patients. We extracted 119 PA view X-ray images of normal patients. In total, our dataset has 239 images with 120 from COVID-19 patients and 119 from normal patients.

3.1 Dataset Statistics

Having a wide distribution within a dataset is an important factor for training a deep learning model since training on narrowly distributed data may lead to a biased model due to a failure to generalize the classification features. Figure 3 depicts our dataset distribution, with respect to location, gender and age of patients. The figure shows that our image collection comes from 62 male and 39 female patients spread across twelve countries, and that their age is normally distributed but shifted towards elderly patients. A patient’s ethnicity was not made public.

Age: The dataset has patients from age 12 to 84, with an average age of 57.33 years. Figure 3a shows the count of samples in the age category and the gender count in each category. Our dataset has a wide range of patients in terms of their ages.

Location: Figure 3b shows the location of patients. The location is an important attribute since a model trained on data from only one country may become biased. Greater variation in the training data can help generalize a deep learning model. Our dataset has images of patients from twelve countries.

3.2 UMAP Exploration

We applied the Uniform Manifold Approximation and Projection (UMAP) technique, which is a non-linear dimensionality reduction technique, to the images. The feature space of UMAP is found by searching for a low dimensional projection of data which is the closest equivalent to the real data using a fuzzy topological structure. We prepared the dataset for UMAP by performing a standard image pre-processing of all images, as described further in Section 5.1. We replaced every image with its zoomed (30%) image. Figure 2 shows the result of the UMAP. In the figure the X-ray of a normal patient

²<https://www.sirm.org/category/senza-categoria/covid-19/>

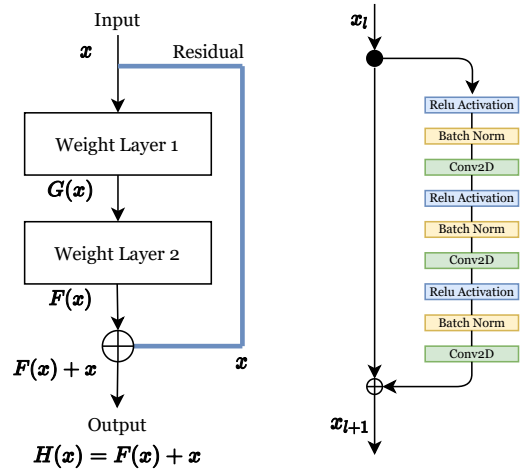


Figure 4: Image on the left shows a Residual block and on the right shows full pre-activation used as our Residual block

has a green bounding box while that of a COVID-19 patient has a red bounding box. The figure shows two clusters, one dominated by COVID-19 images, the other by normal images.

4 APPROACH

In this section, we explain Residual block, Attention block and how we used them to build a Residual Attention Network, which extends the original Residual Attention Network [38].

4.1 Residual Block

Deep convolution networks have revolutionized the field of image classification. Advancements in algorithms and hardware networks have increased the ability to add layers to a deep convolution network, but with the increase in the depth of the network it becomes harder to train a neural network because of vanishing gradients. Networks with too many layers become highly unstable as the value of gradients approaches zero in early layers and with every additional layer gradient values become smaller and eventually insignificant. Vanishing gradients degrade the performance of the network and adding more layers only exacerbates the problem. To solve the vanishing gradient problem Kaiming He et al. [14] proposed *residual connections*. A residual connection merges the output of a layer with the input of a previous layer, which ensures that gradient values do not suddenly vanish. A residual connection acts like insurance for the value of gradients. As shown in Figure 4 on the left is a residual block with a residual connection.

A deep learning model in general tries to learn a mapping function $H(x)$ from an input x to output y ,

$$H(x) = y \quad (1)$$

In a residual block, instead of learning a direct mapping it uses the difference between the mapping of x and the original input x ,

$$F(x) = H(x) - x \quad (2)$$

re-arranging gives,

$$H(x) = F(x) + x \quad (3)$$

residual block learns the residual $F(x)$ with given x as an input and $H(x)$ as the true output. This technique helps when increasing the depth of a neural network.

Our experiments with arranging residual block for optimal gradient flow showed full pre-activation with batch normalization gives the best results, which was also suggested by Kaiming He et al. [14]. Our full pre-activation block is shown in the right of Figure 4, where we use Relu activation, batch normalization and a 2D convolution layer stacked three times. The sequence and stacking of our block is different than originally proposed, which was batch normalization, Relu activation and convolution layer stacked twice. From our experiments we observed that batch normalization after Relu activation performs better. The reason for better performance happened when input features x were negative, in the network they would have been truncated using non-linearity activation function Relu before batch normalization. Performing batch normalization prior to Relu activation will include these negative values in feature space.

4.2 Attention Block

The attention mechanism has become a very popular technique in natural language processing, image processing and computer vision. Attention mechanism can generate attention-aware features and features could be extracted based on spatial, context or channel aware-features. It also learns the importance and correlations among features. Using a visual attention in an image classification task helps determine important image regions and their correlations. The presence or absence of image regions is critical to classification. In our case these regions are evidence of COVID-19 infection in chest X-ray images. Our attention module consists of two branches a “trunk” branch $T(x)$ with two stacked residual blocks and an hourglass encoder-decoder “mask” branch $M(x)$.

The mask branch contains an encoder and decoder, where an encoder consist of downsampling using max pooling followed by residual connection and downsampling again. The encoder acts as an input reducer. The decoder consists of upsampling using bilinear interpolation. In the original Residual Attention Network there is only one upsample but in a literature survey we found that the performance of a Residual Attention Network can be increased by increasing the number of up-sampling layers [?]. We extended the Attention block by adding two upsample layers in our model. The encoder and decoder are followed by two convolution layers and a sigmoid activation as displayed in Figure 5. The trunk branch consists of two stacked residual blocks which perform feature processing.

The final output of the module is

$$F(x) = (1 + M(x)) * T(x) \quad (4)$$

adding 1 to the equation ensures that in case of mask branch with zero output the trunk branch computation passes through, which dampens the susceptibility to noisy data.

4.3 Residual Attention Network

Previously we described our unit modules Residual block and Attention block, our Residual Attention Network is built by multiple

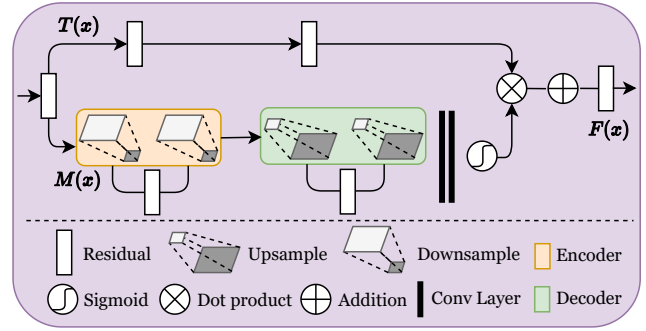


Figure 5: Design of Attention Block

stacking of our basic unit module. The stacking of blocks is designed for optimal performance and to prevent overfitting. The Attention block is designed to explore fine-grained feature maps, since COVID-19 infections could be a fine detail in an X-ray. There are two major attention categories: *Soft* and *Hard*, we use *Soft* attention to learn alignment for several patches and *Hard* attention to learn only one patch at a time.

The Residual block captures high-level features and provides input to an Attention block. The Attention module generates specialized low-level features on each Residual input. It divides an image into a few high-level features and from those features extracts several low-level features. We stack Residual and Attention layers alternatively three times. The Residual layer extracts high-level features from the input image which are then passed to the Attention block, which extracts low-level features. These low-level features become input to next Residual block in turn. It works as both a top-down and bottom-up approach, the top-down network produces dense features and the bottom-up one produces low resolution feature maps. This technique has proved successful in image segmentation [?]. Our scenario is very similar to segmentation where we try to identify low-level patches of COVID-19 infections in a chest X-ray. Our architecture is shown in Table 1, which modifies [38] with several fundamental modifications (kernel sizes, output head, channels, pooling size) for optimal performance.

5 EXPERIMENTS

This section presents an experimental evaluation of our model. We start with data preprocessing and data splits for training, testing and validation. We describe the experimental setup, our models and their configurations, and we show results.

5.1 Data Preprocessing

Data preprocessing plays an important role in training a deep learning model. Previous research has highlighted the impact of preprocessing on model performance [?]. Images in our dataset have different sizes, so we first start with standardizing the image size to 224 x 224 pixels. The collected images also have different color patterns, so we normalize the color pattern to RGB. Lastly, we normalize the maximum intensity of a pixel to 255 (lowest is 0). Our dataset has two different classes, labelled *COVID* and *Normal*; during training we use a label binarizer to convert them to one-hot encoding.

Layers	Output Size	Kernel Size
Convolution 2D	112×112	(5×5), p =same
MaxPool 2D	56×56	(2×2), 2
Residual Block	56×56	$\begin{pmatrix} 1 \times 1 & 32 \\ 3 \times 3 & 32 \\ 1 \times 1 & 128 \end{pmatrix}$
Attention Block	56×56	Attention×1
Residual Block	28×28	$\begin{pmatrix} 1 \times 1 & 128 \\ 3 \times 3 & 128 \\ 1 \times 1 & 256 \end{pmatrix}$
Attention Block	28×28	Attention×1
Residual Block	14×14	$\begin{pmatrix} 1 \times 1 & 256 \\ 3 \times 3 & 256 \\ 1 \times 1 & 512 \end{pmatrix}$
Attention Block	14×14	Attention×1
Residual Block	7×7	$\begin{pmatrix} 1 \times 1 & 512 \\ 3 \times 3 & 512 \\ 1 \times 1 & 1024 \end{pmatrix}$
Residual Block	7×7	$\begin{pmatrix} 1 \times 1 & 1024 \\ 3 \times 3 & 1024 \\ 1 \times 1 & 1024 \end{pmatrix}$
Residual Block	7×7	$\begin{pmatrix} 1 \times 1 & 1024 \\ 3 \times 3 & 1024 \\ 1 \times 1 & 1024 \end{pmatrix}$
AvgPooling 2D	1×1	(7×7)
FC, Softmax		2
Depth		115

Table 1: Residual Attention Network architecture

5.1.1 Data Split. The dataset is split into training (70%), testing (20%) and validation (10%) sets. We use stratified splits which ensures that each split has an equal number of samples from each class as shown in Table 2. We also add a random rotation of 15° to images, which adds more stability to our model during training.

	COVID	Normal	Total
Train	84	83	167
Test	25	25	50
Validate	11	11	22
	120	119	239

Table 2: COVID dataset splits using Stratified sampling

5.2 Experimental setup

All experiments were carried out on a computer with Intel i7 5820k, Nvidia 1080 ti, 16GB of RAM running Ubuntu 18.04 OS. We use Python 3.7 and its libraries (sklearn, tensorflow, keras) to write and train the deep learning models. All of the networks were trained on Nvidia 1080 ti (3584 CUDA cores and 11GB DDR5 RAM) with CUDA and cuDNN configured for performance enhancement.

5.2.1 Evaluation Metric. To evaluate the performance of our models we use the most commonly used performance metrics for deep learning, namely, sensitivity, specificity, precision, recall and accuracy. Their value range is [0, 1], higher is better. The metrics are given below, where TP is true positive, FP is false positive, TN

is true negative, and FN is false negative.

$$\begin{aligned} \text{sensitivity} &= \frac{TP}{TP + FN} \\ \text{specificity} &= \frac{TN}{FP + TN} \\ \text{precision} &= \frac{TP}{TP + FP} \\ \text{recall} &= \frac{TP}{TP + FN} \\ \text{accuracy} &= \frac{TP + TN}{TP + FP + TN + FN} \end{aligned}$$

5.2.2 Models configuration. We use several popular deep learning models namely VGG, Inception, Xception DenseNet, MobileNet as benchmarks to compare our Residual Attention Network model, as shown in Table 3. Our selection of model size ranges from 15 layers to 270 layers deep. We trained each model with an initial learning rate of 1e−4 and a mini-batch size of 8 with 100 epochs. We used Adam as our optimizer. The Adam optimizer uses two popular optimization techniques, Root Mean Square Propagation (RMSprop) and Stochastic Gradient Descent (SGD) with momentum. To provide stability during training of our models we used a learning rate decay with the decay rate shown in Equation 5. We also randomly rotated images by 15°. During the training, we used Binary Cross entropy as the loss function for all of the models expressed in Equation 6. For our benchmark models, we ran them with pre-trained weights using *imagenet*, which contains 14 million images with over 1000 classes. Training on a large dataset requires massive computational power, for example NASNetLarge was trained using 500 GPUS for four days on the *imagenet* dataset. We used the weights of models after the training and retrained them on our dataset, this methodology is commonly known as *transfer learning*.

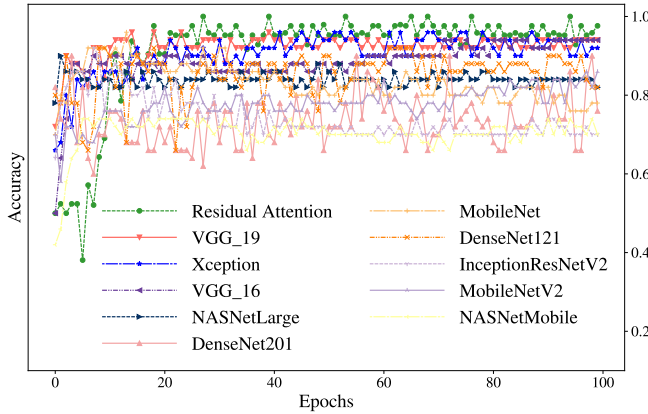
$$\text{Decay Rate} = \frac{\text{Initial Learning Rate}}{\text{Epochs}} \quad (5)$$

$$H_y(p) = - \sum_{i=1}^n (y_i \log(p) + (1 - y_i) \log(1 - p)) \quad (6)$$

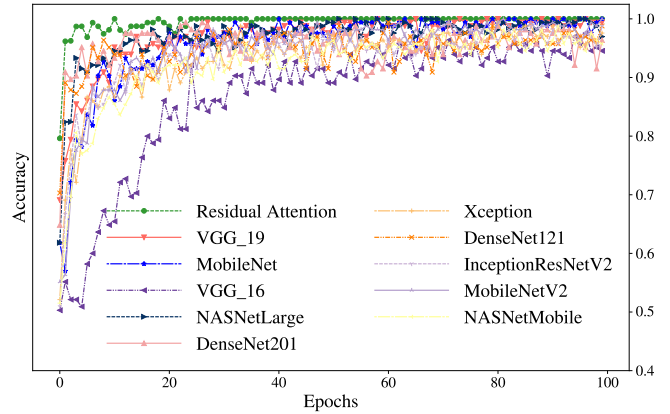
5.2.3 Output head modification. The predefined models have been designed and trained for the very large *imagenet* dataset consisting of 1000 classes and millions of images whereas our dataset has two classes and 239 images. To prevent overfitting of the predefined models on our small dataset, we modified the output layers of all of the models. We removed the output layer and added a custom output head. For example, VGG16 has three fully connected layers as the output head, the first two layers have 4096 neurons while the third has 1000 (number of classes) neurons. We modified this output from three layers to two layers with 64 neurons in the first layer and 2 (number of classes) neurons in second layer. This reduces the number of layers by one for each of the predefined models as shown in Table 3. We did this on all of the models to standardize the output head.

5.3 Results

Table 4 displays the accuracy of the models on the testing and validation sets of our COVID-19 dataset. We observe that the Residual Attention Network outperforms all other deep learning models,



Accuracy over epochs of models on testing set



Accuracy over epochs of models on training set

Figure 6: Training and testing accuracy for all models

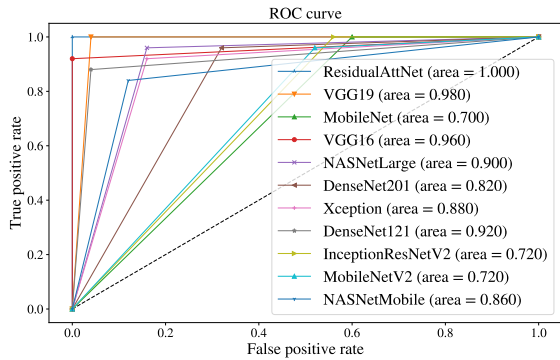


Figure 7: ROC curves and AUC value for all models. Our prediction has only two classes, we have only 3 thresholds [2,1,0] for ROC curve. AUC values are quantified in the legend

	Layers	Batch Size	Channel	Epochs
VGG16	15	8	3	100
VGG19	18	8	3	100
MobileNet	29	8	3	100
Xception	42	8	3	100
MobileNetV2	54	8	3	100
Residual Network	115	8	3	100
DenseNet121	122	8	3	100
NASNetMobile	198	8	3	100
DenseNet201	202	8	3	100
InceptionResNetV2	246	8	3	100
NASNetLarge	270	8	3	100

Table 3: Configurations of models

while NASNetMobile turns out to be the worst performer. Our experiments show that VGG19 performs better than VGG16. Even though both models are similar, VGG19 has more layers and it is commonly thought that deeper pretrained models perform better than shallower models. But that is not the case for our dataset, for instance the network with shallower depth, DenseNet121, performed

better than a very deep network, DenseNet201 (both networks are at least six times deeper than VGG19). From this we observe that it boils down to feature maps of layers from a model, which is dependent on the convolution layers. We also observe that very deep networks do not perform better than shallower ones since the top two performing networks are shallow networks (1/4 of the size of the largest network). Figure 6 shows the model accuracy for every epoch. We observe large/deeper models (DenseNet201, NASNetLarge, InceptionResNetV2) tend to overfit and shallower models (VGG16, VGG19, Residual Attention Network) are able to generalize our dataset better.

Overall our experiments show that the Residual Attention Network performs best with 98% accuracy on testing and 100% on validation set to detect COVID-19 in X-ray images.

5.3.1 COVID-19 prediction explanation. Figure 8 visualizes the feature maps of the first two layers of our Residual Attention Network model trained on our COVID-19 dataset. There are 64 images in each picture with an 8x8 grid for each individual image. The feature maps were generated by passing an image to our trained model and collecting data of activated neurons, basically outputs of the first convolution layer and pooling layer. We select only the first two layers and 64 neurons of each layer since the number of neurons and parameters grows exponentially at every layer. We observe from the feature maps of both layers that our model is able to extract relevant details from an image, e.g., lungs, spine, veins, all potential COVID-19 affected areas.

6 CONCLUSION

The paper proposes a novel method to detect COVID-19 using chest X-ray images. The method uses a Residual Attention Network and data augmentation. We collected and curated a dataset of 239 images, 120 images of patients infected with COVID-19 and 119 images of non-COVID-19 patients, which we label “normal.” The dataset is diverse in terms of patient age, gender and location. We applied a non-linear dimensionality reduction technique, UMAP, and observed a clear distinction between X-rays of COVID-19 and

Network	Testing Set						Validation Set					
	Sensitivity	Specificity	Precision	Recall	Accuracy	AUC	Sensitivity	Specificity	Precision	Recall	Accuracy	Error (95% CI)
NASNetMobile	0.72	0.68	0.69	0.70	0.7000	0.86	0.82	0.55	0.64	0.75	0.6818	(0.0, 0.24)
MobileNetV2	0.72	1.00	1.00	0.78	0.8600	0.72	0.55	0.91	0.86	0.67	0.7273	(0.0, 0.21)
InceptionResNetV2	0.40	1.00	1.00	0.63	0.7000	0.72	0.55	1.00	1.00	0.69	0.7727	(0.0, 0.18)
DenseNet121	0.92	0.72	0.77	0.90	0.8200	0.92	0.82	0.82	0.82	0.82	0.8182	(0.0, 0.06)
Xception	0.84	1.00	1.00	0.86	0.9200	0.88	0.91	0.82	0.83	0.90	0.8636	(0.0, 0.13)
DenseNet201	0.52	1.00	1.00	0.68	0.7600	0.82	0.82	0.91	0.90	0.83	0.8636	(0.0, 0.13)
NASNetLarge	0.72	0.92	0.90	0.77	0.8200	0.90	0.82	0.91	0.90	0.83	0.8636	(0.0, 0.13)
VGG16	1.00	0.88	0.89	1.00	0.9400	0.96	1.00	0.82	0.85	1.00	0.9091	(0.0, 0.09)
MobileNet	0.56	1.00	1.00	0.69	0.7800	0.70	0.82	1.00	1.00	0.85	0.9091	(0.0, 0.09)
VGG19	0.96	0.92	0.92	0.96	0.9400	0.98	0.92	1.00	1.00	0.92	0.9545	(0.0, 0.06)
Residual Att Net	1.00	0.96	0.96	1.00	0.9800	1.00	1.00	1.00	1.00	1.00	1.0000	(0.0, 0.00)

Table 4: Sensitivity, Specificity and Accuracy from all models on Testing and Validation set

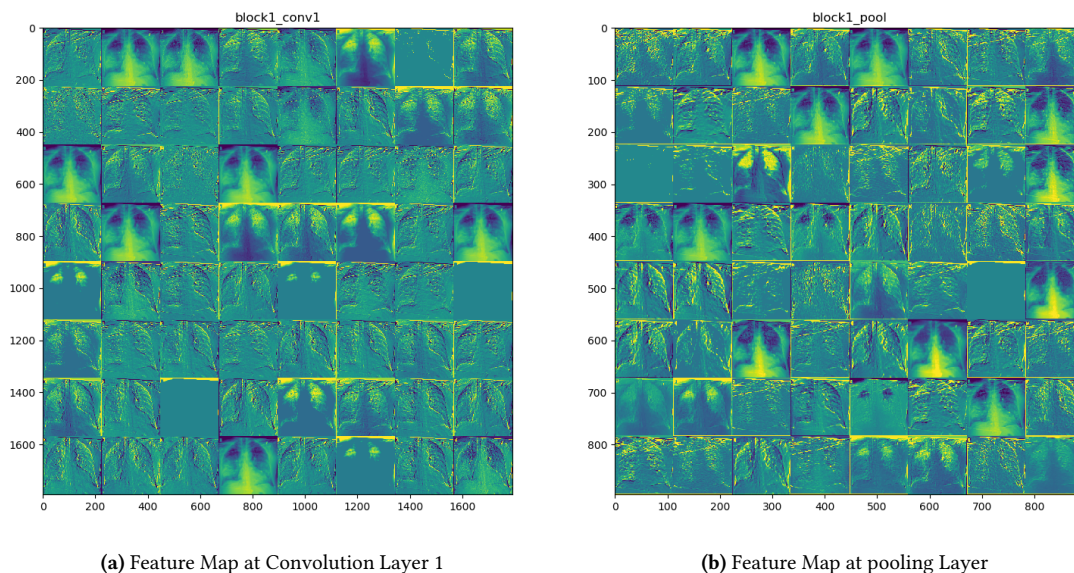


Figure 8: Feature maps of Residual Attention Network at first 2 Layers

normal patients. We designed and implemented a Residual Attention Network to classify COVID-19 patients and compared our model with many popular deep learning models: VGG, DenseNet, NASNet, Xception, and Inception. Our experiments show that our Residual Attention Network performs best among all of the models with 98% testing and 100% validation accuracy. We generated feature maps of the Residual Attention Network and they show that the low-level features extracted from a given image include areas of potential COVID-19 infection.

This applied research shows that chest X-ray images can potentially be used to detect COVID-19, or can be combined with other testing methods to corroborate a diagnostic outcome. The immediate future work is to add more images to our dataset. A second avenue of future work is to work with domain experts to study the utility of deploying the technique in practice, due to the recent nature of the COVID-19 pandemic, the deployment has lagged

behind the applied research. Another aspect of future work is to study whether chest X-rays can be used to detect COVID-19 early in the illness or in asymptomatic cases. Our X-ray dataset does not have information about patient symptoms or time with the disease, only that the X-rays are of COVID-19 positive patients. Since early detection is important to effective quarantining, it would be interesting to test our model on X-rays from patients who have just been infected or who are asymptomatic.

REFERENCES

- [1] Tao Ai, Zhenlu Yang, Hongyan Hou, Chenao Zhan, Chong Chen, Wenzhi Lv, Qian Tao, Ziyong Sun, and Liming Xia. 2020. Correlation of Chest CT and RT-PCR Testing in Coronavirus Disease 2019 (COVID-19) in China: A Report of 1014 Cases. *Radiology* (2020), 200642. <https://doi.org/10.1148/radiol.2020200642> PMID: 32101510.
- [2] Ali Mohammad Alqudah, Shoroq Qazan, Hiam Alquran, Isam Abu Qasmieh, and Amin Alqudah. 2020. Covid-2019 Detection Using XRay Images And Artificial Intelligence Hybrid Systems. (2020).

- [3] Khalid El Asnaoui, Youness Chawki, and Ali Idri. 2020. Automated methods for detection and classification pneumonia based on x-ray images using deep learning. *arXiv preprint arXiv:2003.14363* (2020).
- [4] Vijay Badrinarayanan, Alex Kendall, and Roberto Cipolla. 2017. Segnet: A deep convolutional encoder-decoder architecture for image segmentation. *IEEE transactions on pattern analysis and machine intelligence* 39, 12 (2017), 2481–2495.
- [5] Dzmitry Bahdanau, Kyunghyun Cho, and Yoshua Bengio. 2014. Neural Machine Translation by Jointly Learning to Align and Translate. (2014). arXiv:cs.CL/1409.0473
- [6] Mucahid Barstugan, Umur Ozkaya, and Saban Ozturk. 2020. Coronavirus (covid-19) classification using ct images by machine learning methods. *arXiv preprint arXiv:2003.09424* (2020).
- [7] Charmaine Butt, Jagpal Gill, David Chun, and Benson A Babu. 2020. Deep learning system to screen coronavirus disease 2019 pneumonia. *Applied Intelligence* (2020), 1.
- [8] Jun Chen, Lianlian Wu, Jun Zhang, Liang Zhang, Dexin Gong, Yilin Zhao, Shan Hu, Yonggui Wang, Xiao Hu, Biqing Zheng, et al. 2020. Deep learning-based model for detecting 2019 novel coronavirus pneumonia on high-resolution computed tomography: a prospective study. *medRxiv* (2020).
- [9] François Chollet. 2017. Xception: Deep learning with depthwise separable convolutions. In *Proceedings of the IEEE conference on computer vision and pattern recognition*. 1251–1258.
- [10] Joseph Paul Cohen, Paul Morrison, and Lan Dao. 2020. COVID-19 image data collection. *arXiv 2003.11597* (2020). <https://github.com/ieee8023/covid-chestxray-dataset>
- [11] Joseph Paul Cohen, Paul Morrison, and Lan Dao. 2020. COVID-19 image data collection. *arXiv 2003.11597* (2020). <https://github.com/ieee8023/covid-chestxray-dataset>
- [12] George E Dahl, Dong Yu, Li Deng, and Alex Acero. 2011. Context-dependent pre-trained deep neural networks for large-vocabulary speech recognition. *IEEE Transactions on audio, speech, and language processing* 20, 1 (2011), 30–42.
- [13] Ophir Gozes, Maayan Frid-Adar, Nimrod Sagie, Huangqi Zhang, Wenbin Ji, and Hayit Greenspan. 2020. Coronavirus detection and analysis on chest ct with deep learning. *arXiv preprint arXiv:2004.02640* (2020).
- [14] Kaiming He, Xiangyu Zhang, Shaoqing Ren, and Jian Sun. 2015. Deep Residual Learning for Image Recognition. *CoRR abs/1512.03385* (2015). arXiv:1512.03385 <http://arxiv.org/abs/1512.03385>
- [15] Andrew G Howard, Menglong Zhu, Bo Chen, Dmitry Kalenichenko, Weijun Wang, Tobias Weyand, Marco Andreetto, and Hartwig Adam. 2017. MobileNets: Efficient convolutional neural networks for mobile vision applications. *arXiv preprint arXiv:1704.04861* (2017).
- [16] Gao Huang, Zhuang Liu, and Kilian Q Weinberger. 2016. Densely Connected Convolutional Networks. *CoRR abs/1608.06993* (2016). arXiv:1608.06993 <http://arxiv.org/abs/1608.06993>
- [17] Zixing Huang, Shuang Zhao, Zhenlin Li, Weixia Chen, Lihong Zhao, Lipeng Deng, and Bin Song. 2020. The Battle Against Coronavirus Disease 2019 (COVID-19): Emergency Management and Infection Control in a Radiology Department. *Journal of the American College of Radiology* (2020). <https://doi.org/10.1016/j.jacr.2020.03.011>
- [18] Baris Kayalibay, Grady Jensen, and Patrick van der Smagt. 2017. CNN-based segmentation of medical imaging data. *arXiv preprint arXiv:1701.03056* (2017).
- [19] Alex Krizhevsky, Ilya Sutskever, and Geoffrey E Hinton. 2012. Imagenet classification with deep convolutional neural networks. In *Advances in neural information processing systems*. 1097–1105.
- [20] Lin Li, Lixin Qin, Zeguo Xu, Youbing Yin, Xin Wang, Bin Kong, Junjie Bai, Yi Lu, Zhenghan Fang, Qi Song, et al. 2020. Artificial intelligence distinguishes COVID-19 from community acquired pneumonia on chest CT. *Radiology* (2020), 200905.
- [21] Qing Li, Weidong Cai, Xiaogang Wang, Yun Zhou, David Dagan Feng, and Mei Chen. 2014. Medical image classification with convolutional neural network. (2014), 844–848.
- [22] Xin Li and Dongxiao Zhu. 2020. Covid-xpert: An ai powered population screening of covid-19 cases using chest radiography images. *arXiv preprint arXiv:2004.03042* (2020).
- [23] Shuying Liu and Weihong Deng. 2015. Very deep convolutional neural network based image classification using small training sample size. In *2015 3rd IAPR Asian conference on pattern recognition (ACPR)*. IEEE, 730–734.
- [24] Kelly Geraldine Malone. March 25, 2020. *Testing backlog linked to shortage of chemicals needed for covid-19 test*. <https://bit.ly/2SEXzVY>
- [25] Paul Mooney. June 2019. *Chest X-Ray Images (Pneumonia)*. <https://www.kaggle.com/paultimothymooney/chest-xray-pneumonia>
- [26] Ali Narin, Ceren Kaya, and Ziynet Pamuk. 2020. Automatic detection of coronavirus disease (covid-19) using x-ray images and deep convolutional neural networks. *arXiv preprint arXiv:2003.10849* (2020).
- [27] World Health Organization. 2004. *Summary of probable SARS cases with onset of illness from 1 November 2002 to 31 July 2003*. https://www.who.int/csr/sars/country/table2004_04_21/en/
- [28] World Health Organization. 2013. *Middle East respiratory syndrome coronavirus (MERS-CoV)*. <https://www.who.int/emergencies/mers-cov/en/>
- [29] MIT Technology Review. 2020. Over 24,000 coronavirus research papers are now available in one place. (2020). <https://www.technologyreview.com/2020/03/16/905290/coronavirus-24000-research-papers-available-open-data/>
- [30] Muhammad Shereen, Suliman Khan, Abeer Kazmi, Nadia Bashir, and Rabea Siddique. 2020. COVID-19 infection: Origin, transmission, and characteristics of human coronaviruses. *Journal of Advanced Research* 24 (03 2020). <https://doi.org/10.1016/j.jare.2020.03.005>
- [31] Feng Shi, Jun Wang, Jun Shi, Ziyang Wu, Qian Wang, Zhenyu Tang, Kelei He, Yinghuan Shi, and Dinggang Shen. 2020. Review of artificial intelligence techniques in imaging data acquisition, segmentation and diagnosis for covid-19. *IEEE Reviews in Biomedical Engineering* (2020).
- [32] Tanu Singhal. 2020. A Review of Coronavirus Disease-2019 (COVID-19). *The Indian Journal of Pediatrics* 87 (03 2020). <https://doi.org/10.1007/s12098-020-03263-6>
- [33] Sanche Steven, Yen Ting Lin, Chonggang Xu, Ethan Romero-Severson, Nick Hengartner, and Ruian Ke. 2020. High Contagiousness and Rapid Spread of Severe Acute Respiratory Syndrome Coronavirus 2. In *Center for Disease Control and Prevention (CDC)*. <https://doi.org/10.3201/eid2607.200282>
- [34] Christian Szegedy, Wei Liu, Yangqing Jia, Pierre Sermanet, Scott E. Reed, Dragomir Anguelov, Dumitru Erhan, Vincent Vanhoucke, and Andrew Rabinovich. 2014. Going Deeper with Convolutions. *CoRR abs/1409.4842* (2014). arXiv:1409.4842 <http://arxiv.org/abs/1409.4842>
- [35] Christian Szegedy, Alexander Toshev, and Dumitru Erhan. 2013. Deep neural networks for object detection. In *Advances in neural information processing systems*. 2553–2561.
- [36] John Hopkins University and Medicine. 2020. *Coronavirus resource center*. <https://coronavirus.jhu.edu/us-map>
- [37] Ashish Vaswani, Noam Shazeer, Niki Parmar, Jakob Uszkoreit, Llion Jones, Aidan N Gomez, Łukasz Kaiser, and Illia Polosukhin. 2017. Attention is all you need. In *Advances in neural information processing systems*. 5998–6008.
- [38] Fei Wang, Mengqing Jiang, Chen Qian, Shuo Yang, Cheng Li, Honggang Zhang, Xiaogang Wang, and Xiaoou Tang. 2017. Residual attention network for image classification. In *Proceedings of the IEEE Conference on Computer Vision and Pattern Recognition*. 3156–3164.
- [39] Shuai Wang, Bo Kang, Jinlu Ma, Xianjun Zeng, Mingming Xiao, Jia Guo, Mengjiao Cai, Jingyi Yang, Yaodong Li, Xiangfei Meng, et al. 2020. A deep learning algorithm using CT images to screen for Corona Virus Disease (COVID-19). *MedRxiv* (2020).
- [40] Shuai Wang, Bo Kang, Jinlu Ma, Xianjun Zeng, Mingming Xiao, Jia Guo, Mengjiao Cai, Jingyi Yang, Yaodong Li, Xiangfei Meng, and Bo Xu. 2020. A deep learning algorithm using CT images to screen for Corona Virus Disease (COVID-19). *medRxiv* (2020). <https://doi.org/10.1101/2020.02.14.20023028>
- [41] Yu-Huan Wu, Shang-Hua Gao, Jie Mei, Jun Xu, Deng-Ping Fan, Chao-Wei Zhao, and Ming-Ming Cheng. 2020. JCS: An Explainable COVID-19 Diagnosis System by Joint Classification and Segmentation. (2020). arXiv:ess.IV/2004.07054
- [42] Laure Wynants, Ben Van Calster, Marc MJ Bonten, Gary S Collins, Thomas PA De-bray, Maarten De Vos, Maria C Haller, Georg Heinze, Karel GM Moons, Richard D Riley, et al. 2020. Prediction models for diagnosis and prognosis of covid-19 infection: systematic review and critical appraisal. *bmj* 369 (2020).
- [43] Xiaowei Xu, Xiangao Jiang, Chunlian Ma, Peng Du, Xukun Li, Shuangzhi Lv, Liang Yu, Yanfei Chen, Junwei Su, Guanqing Lang, Yongtao Li, Hong Zhao, Kaijin Xu, Lingxiang Ruan, and Wei Wu. 2020. Deep Learning System to Screen Coronavirus Disease 2019 Pneumonia. (2020). arXiv:physics.med-ph/2002.09334
- [44] Jason Yosinski, Jeff Clune, Yoshua Bengio, and Hod Lipson. 2014. How transferable are features in deep neural networks?. In *Advances in neural information processing systems*. 3320–3328.
- [45] Han Zhang, Ian Goodfellow, Dimitris Metaxas, and Augustus Odena. 2018. Self-Attention Generative Adversarial Networks. (2018). arXiv:stat.ML/1805.08318
- [46] Jianpeng Zhang, Yutong Xie, Yi Li, Chunhua Shen, and Yong Xia. 2020. Covid-19 screening on chest x-ray images using deep learning based anomaly detection. *arXiv preprint arXiv:2003.12338* (2020).
- [47] Zongwei Zhou, Md Mahfuzur Rahman Siddiquee, Nima Tajbakhsh, and Jianming Liang. 2018. U-Net++: A Nested U-Net Architecture for Medical Image Segmentation. *CoRR abs/1807.10165* (2018). arXiv:1807.10165 <http://arxiv.org/abs/1807.10165>